UNIVERSITÄT BASEL

UNIVERSITÄTSBIBLIOTHEK

edoc

Institutional Repository of the University of Basel
University Library
Schoenbeinstrasse 18-20
CH-4056 Basel, Switzerland
http://edoc.unibas.ch/

UB | Für alle offen

Year: 2013

The transcriptional coactivator PGC-1α is dispensable for chronic overload-induced skeletal muscle hypertrophy and metabolic remodeling

Pérez-Schindler, Joaquín and Summermatter, Serge and Santos, Gesa and Zorzato, Francesco and Handschin, Christoph

Posted at edoc, University of Basel

Official URL: http://edoc.unibas.ch/dok/A6205557

Originally published as:

Pérez-Schindler, Joaquín and Summermatter, Serge and Santos, Gesa and Zorzato, Francesco and Handschin, Christoph. (2013) *The transcriptional coactivator PGC-1α is dispensable for chronic overload-induced skeletal muscle hypertrophy and metabolic remodeling.* Proceedings of the National Academy of Sciences of the United States of America, Vol. 110, H. 50. S. 20314-20319.

UNI BASEL

PGC-1α Is Dispensable for Chronic Overload-Induced Skeletal Muscle Hypertrophy and Metabolic Remodeling

Joaquín Pérez-Schindler[a], Serge Summermatter[a,1], Gesa Santos[a], Francesco Zorzato[b,c], and Christoph Handschin[a,2]

[a]Biozentrum, University of Basel, Klingelbergstrasse 50/70, 4056 Basel, Switzerland; [b]Departments of Anesthesia and Biomedicine, Basel University Hospital, Hebelstrasse 20, 4031 Basel, Switzerland; [c]Department of Experimental and Diagnostic Medicine, University of Ferrara, Via Borsari 46, 44100 Ferrara, Italy

Published in Proc Natl Acad Sci U S A. 2013 Dec 10;110(50):20314-9. PMID: 24277823. doi: 10.1073/pnas.1312039110

Copyright © National Academy of Sciences; Proceedings of the National Academy of Sciences USA

PGC-1α Is Dispensable for Chronic Overload-Induced Skeletal Muscle Hypertrophy and Metabolic Remodeling

Joaquín Pérez-Schindler[a], Serge Summermatter[a,1], Gesa Santos[a], Francesco Zorzato[b,c], and Christoph Handschin[a,2]

[a]Biozentrum, University of Basel, Klingelbergstrasse 50/70, 4056 Basel, Switzerland; [b]Departments of Anesthesia and Biomedicine, Basel University Hospital, Hebelstrasse 20, 4031 Basel, Switzerland; [c]Department of Experimental and Diagnostic Medicine, University of Ferrara, Via Borsari 46, 44100 Ferrara, Italy

[1]Current address: Novartis Institute for Biomedical Research, Fabrikstrasse 28, 4056 Basel, Switzerland

[2]Corresponding author: Christoph Handschin, Biozentrum, University of Basel, Klingelbergstrasse 50/70, 4056 Basel, Switzerland. Phone: +41 61 267 2378, e-mail: christoph.handschin@unibas.ch

Author contributions: J.P.S. and C.H. designed research; J.P.S., S.S., G.S., and F.Z. performed research; J.P.S., S.S., F.Z., and C.H. analyzed data; J.P.S. and C.H. wrote the paper.

Major category: Biological Sciences

Minor category: Physiology

Keywords: skeletal muscle hypertrophy, skeletal muscle remodeling, energy metabolism

Abstract

Skeletal muscle mass loss and dysfunction have been linked to many diseases. Inversely, resistance exercise, mainly by activating mammalian target of rapamycin complex 1 (mTORC1), promotes skeletal muscle hypertrophy and exerts several therapeutic effects. Moreover, mTORC1, along with peroxisome proliferator-activated receptor γ coactivator 1α (PGC-1α), regulates skeletal muscle metabolism. However, it is unclear whether PGC-1α is required for skeletal muscle adaptations following overload. Here, we show that while chronic overload of skeletal muscle via synergist ablation (SA) strongly induces hypertrophy and a switch toward a slow-contractile phenotype, these effects were independent of PGC-1α. In fact, SA down-regulated PGC-1α expression and led to a repression of energy metabolism. Interestingly however, PGC-1α deletion preserved peak force after SA. Taken together, our data suggest that PGC-1α is not involved in skeletal muscle remodeling induced by SA.

Significance Statement

Skeletal muscle hypertrophy is mainly induced by growth hormones and mechanical overload and exerts health beneficial effects. The mammalian target of rapamycin complex 1 (mTORC1) and the peroxisome proliferator-activated receptor γ coactivator 1α (PGC-1α) are key regulators of skeletal muscle mass and energy metabolism, respectively. Thus, acting in concert, mTORC1 and PGC-1α interplay is thought to regulate skeletal muscle function. Our results indicate now that PGC-1α is not required for skeletal muscle hypertrophy and a slow-contractile phenotype induced by chronic overload of the plantaris muscle. In fact, PGC-1α gene expression and global energy metabolism were repressed in this experimental context of muscle hypertrophy. Hence, these results exclude PGC-1α as the main regulator of skeletal muscle remodeling following chronic overload.

Introduction

Skeletal muscle size exhibits drastic changes throughout life, mainly dependent on mechanical load and nutritional supply (1). For example, loss of muscle mass is observed during immobilization and starvation, but also under pathological conditions like heart failure and cancer (2). To date, resistance exercise is considered as one of the most efficient ways to induce skeletal muscle hypertrophy and to revert the adverse effects of muscle wasting (2, 3). However, since pharmacological interventions are scarce, identification of the molecular regulation of muscle remodeling via resistance exercise is of great therapeutic interest.

Activation of mammalian target of rapamycin complex 1 (mTORC1) is the main regulatory step by which resistance exercise enhances protein synthesis and skeletal muscle size (4). In fact, inhibition of mTORC1 drastically abrogates plantaris hypertrophy via chronic overload (5), even though muscle size is not affected uniformly by muscle knockout of the mTORC1 inhibitor tuberous sclerosis complex 1 (6). Interestingly, the activity of the mTORC1 protein kinase complex positively correlates with oxidative capacity (7, 8). Moreover, mTORC1 is recruited to the promoter of a wide range of metabolism-related genes to regulate their expression (9-11). In skeletal muscle, mTORC1 regulates oxidative metabolism by facilitating the activation of YY1 by the peroxisome proliferator-activated receptor γ coactivator 1α (PGC-1α) (10, 12). The physiological context in which the mTORC1-PGC-1α axis regulates energy metabolism however is unknown.

Protein degradation is an important limiting factor of skeletal muscle hypertrophy. This process is fine-tuned by the transcription factor forkhead box O3 (FOXO3), which regulates the expression of the E3 ubiquitin ligases MuRF1 and F-box protein 32 (Fbxo32/atrogin-1) (13). Interestingly, PGC-1α represses FOXO3 activity and consequently ameliorates skeletal

muscle mass loss during denervation and aging (14-16). Finally, a recently discovered transcript variant of PGC-1α called PGC-1α4 also protects against skeletal muscle wasting and even promotes skeletal muscle hypertrophy (17). Inversely however, the functional requirement for PGC-1α in muscle hypertrophy and its associated adaptations has not been studied so far. Here, we therefore examined the role of PGC-1α in the molecular and functional adaptations to chronic overload of skeletal muscle.

Results

PGC-1α is Not Required For Chronic Overload-Induced Plantaris Hypertrophy. In order to induce skeletal muscle hypertrophy via mechanical overload, we have taken advantage of the well-established method of synergist ablation (SA) (18, 19). The role of PGC-1α in skeletal muscle was studied using wild type (WT), PGC-1α muscle-specific transgenic (mTg) and PGC-1α muscle-specific knockout (mKO) mice (Fig. S1A and B) thereby avoiding confounding factors of whole body KO and Tg models (20). Under basal conditions, neither body weight nor wet weight of gastrocnemius, plantaris, tibialis anterior and quadriceps showed significant differences between genotypes (Table S1). However, soleus was slightly heavier in mTg mice, while extensor digitorum longus (EDL) was slightly lighter in both mTg and mKO animals (Table S1).

Following SA, we observed a ~87% increase in the relative mass of WT and mTg overloaded plantaris (OVL) (Fig. 1A). Interestingly, this response was slightly attenuated in mKO mice (Fig. 1A). Moreover, absolute protein and RNA content were elevated by ~53% and ~63%, respectively, in OVL of all genotypes (Fig. 1B and S1C). Whereas relative RNA content remained higher after SA (Fig. S1D), relative protein content was decreased in WT and mTg OVL (Fig. 1C). All genotypes showed an increase in whole plantaris cross sectional area (CSA) in response to SA (Fig. 1D). The analysis of single muscle fiber CSA also revealed an overall shift towards a higher proportion of large fibers in WT, mTg and mKO OVL (Fig. 1E and F).

Next, plantaris hypertrophy was further studied at the molecular level. Interestingly, relative phosphorylation levels of the mTORC1 target protein ribosomal protein S6 kinase (S6K) were increased and decreased in mTg and mKO control plantaris (CON), respectively (Fig. 1G and S1E). After SA, relative p-S6K^{T389} levels remained elevated in mTg OVL while they significantly increased in WT and mKO mice compared to CON (Fig. 1G and S1E). Surprisingly, this positive

effect on S6K phosphorylation was particularly pronounced in mKO mice (Fig. 1G and S1E). In contrast, relative phosphorylation levels of the mTORC1 and phosphatidylinositol 3-kinase (PI3K) target proteins eukaryotic translation initiation factor 4E binding protein 1 (4E-BP1) and Akt, respectively, were not increased by SA (Fig. 1G and S1E). The total protein content of these proteins was elevated by SA in all genotypes (Fig. 1G and S1F).

Next, transcriptional analysis revealed lower levels of insulin-like growth factor 1 (IGF1) mRNA in mTg and mKO CON, while IGF-1 expression was increased by SA in all genotypes (Fig. 1H). Importantly, PGC-1α4 mRNA levels were significantly decreased in both mTg and mKO CON (Fig. 1H). Unexpectedly, we found that SA decreased PGC-1α4 mRNA levels by 32% in WT mice (Fig. 1H). The analysis of genes involved in muscle atrophy showed lower mRNA content of MuRF1 and myostatin (MSTN) in mTg CON (Fig. 1I). SA down-regulated Fbxo32 and MSTN in all genotypes, but the effect on Fbxo32 was slightly reduced in mKO mice (Fig. 1I). MuRF1 mRNA was also lower in WT and mKO OVL, while expression remained low in mTg OVL (Fig. 1I). Thus, these data suggest that PGC-1α does not modulate the overall effects of SA on plantaris hypertrophy.

Metabolic Remodeling Induced by Chronic Overload. Considering the proposed metabolic role of the mTORC1-PGC-1α axis, we also explored the metabolic adaptations to SA. Most of the genes involved in the electron transport chain (ETC), TCA cycle, β-oxidation and fatty acid transport showed higher mRNA levels in mTg CON, while the opposite effects were observed in mKO CON (Fig. 2A and S2A). Genes involved in glucose and lactate metabolism revealed a different pattern, mainly reflecting an enhanced lactate catabolism in mTg CON (Fig. 2A and S2A). Surprisingly, SA down-regulated most of these genes, regardless of the metabolic function (Fig. 2A and S2A). Protein content of different component of the ETC also showed a similar expression pattern, both under basal conditions and after SA (Fig. 2B and

S2B). To further explore the functional effect of SA on oxidative and glycolytic metabolism, we assessed the enzymatic activities of succinate dehydrogenase (SDH) and phosphofructokinase (PFK), respectively. As expected, SDH and PFK activities were higher and lower in mTg CON, respectively (Fig. 2C and D). Following SA, SDH activity was significantly decreased in all genotypes (Fig. 2C), while PFK activity decreased in WT OVL and showed a trend ($p = 0.075$) towards a reduction in mKO OVL (Fig. 2D). Consistently, NADH staining implied an increase and slight decrease in the proportion of oxidative fibers in mTg and mKO CON, respectively, which was reduced in WT and mTg upon SA (Fig. 2E). Additionally, based on NADH staining, either positive fibers (oxidative) and negative fibers (glycolytic) separately or all muscle fibers collectively showed a similar increase in CSA following SA (Fig. S2C). We also found that SA significantly decreased PGC-1α1 mRNA content by 53% and 44% in WT and mTg OVL, respectively (Fig. 2F), similar to the reduction in PGC-1α4 content (Fig. 1H). Importantly, it should be noted that the genetic ablation of PGC-1α in mKO mice was assessed with primers targeting the floxed region of the gene (exon 3 to 5; PGC-1α e3-5) that is shared in all different PGC-1α isoforms (17). In contrast, since specific detection of PGC-1α1, 2, 3 and 4 relies on amplification of transcript regions outside this deleted area, mRNA is detected in mKO mice with primers that are specific for PGC-1α1 (Fig. 2F). Nevertheless however, due to the knockout strategy aimed at introducing a frame-shift in the gene, no protein will be made from these non-functional transcripts in PGC-1α knockout models (21, 22). In contrast to PGC-1α, no major changes in PGC-1β and PGC-1-related coactivator (PRC) were induced by SA (Fig. 2F). The AMP-activated protein kinase (AMPK) is another key regulator of cellular energy metabolism in various tissues (23). Interestingly, relative phosphorylation levels of AMPK and its target protein acetyl-CoA carboxylase (ACC) were highly increased by SA, while absolute levels of ACC were only

increased in WT OVL (Fig. 2G, S2D and S2E). Our results imply a negative effect of SA on energy metabolism, which appears to be related to the down-regulation of PGC-1α and was consequently attenuated by PGC-1α overexpression.

Functional Adaptations to Chronic Overload. Finally, we investigated the effects of SA on plantaris contractility and fatigue resistance. Peak force in response to a single twitch and tetanic stimulation was lower in mTg CON (Fig. 3A-C). In WT, SA significantly decreased force generation independently of the stimulation pattern, while in mTg mice only twitch force was further decreased (Fig. 3A-C). Surprisingly, force generation did not change in mKO mice after SA (Fig. 3A-C). SA also delayed the contractile kinetics observed in response to tetanic stimulation (Table S2). Furthermore, fatigue resistance was higher in mTg CON and SA significantly improved this parameter in all genotypes (Fig. 3D and E). Thus, the area under the curve (AUC) of the fatigue resistance protocol was increased by SA in all genotypes (Fig. 3F).

The contractile properties of muscle cells are in part determined by the specific expression of genes involved in calcium handling and excitation-contraction (EC) coupling (24, 25). Thus, mTg CON showed a shift toward a slow phenotype, mainly reflected by lower mRNA level of calsequestrin 1 (CSQ1) and myosin heavy chain 2 B (MyHC-2B), in contrast to higher levels of the respective slow isoform of these genes, CSQ2 and MyHC-1 (Fig. 4A and B). On the other hand, mKO CON showed higher mRNA level of CSQ1, sarcoplasmic/endoplasmic reticulum Ca^{2+}-ATPase 1 (SERCA1) and actin alpha 1 (ACTC1) (Fig. 4A and C). In line with the functional analysis, SA induced CSQ2, SERCA2, MyHC-2A, ACTC1 and troponin C1 (TNNC1) gene expression in WT OVL (Fig. 4A-C). Moreover, mRNA level of SERCA1, MyHC-2B, ACTN3 and TNNC2 were lower in WT OVL (Fig. 4A-C). These effects of SA were not substantially altered in mTg or mKO mice (Fig. 4A-C). Importantly, the genes up- and down-regulated by SA are

characteristic of slow- and fast-twitch skeletal muscle, respectively (24, 25). At the protein level, we observed a reduction of MyHC-2B and SERCA1 in mTg CON, while SA strongly decreased MyHC-2B in all genotypes and SERCA1 in WT and mKO OVL, further supporting the functional analysis (Fig. 4D and S3A). We finally analyzed myosin regulatory light chain (MLC) phosphorylation by MLC Kinase 2 (MLCK2), a key process for the potentiation of force generation (26). MLCK2 mRNA content decreased by ~42% in mTg CON and WT OVL (Fig. 4E). In contrast, the effect of SA on MLCK2 mRNA was attenuated in mKO OVL (Fig. 4E), strongly supporting the ex vivo assessment of peak force. Interestingly, while relative levels of p-MLC2$^{T18/S19}$ were lower in mTg mice, the opposite effect was found in mKO CON and OVL (Fig. 4F and S3B). In addition, we observed that MLC2 protein content was strongly reduced in mTg CON and it was increased by SA in mTg and mKO OVL (Fig. 4F and S3C). Thus, taken together, the functional and molecular analysis strongly suggests that SA induces a switch toward a slow-contractile phenotype.

Discussion

Different exercise-based and pharmacological strategies have been proposed to prevent skeletal muscle atrophy under pathological conditions, with mTORC1 activation playing a key role in this process (2, 3). In fact, mTORC1 is a well-known mediator of protein synthesis and cell growth and has recently emerged also as a metabolic regulator (27). The link between mTORC1 and skeletal muscle metabolism is thought to be PGC-1α (10, 12). PGC-1α and PGC-1α4 positively modulate skeletal muscle mass under catabolic conditions (14, 16, 17). However, we have now found that regardless of mTORC1 activity, PGC-1α is not required for skeletal muscle remodeling via chronic overload.

The role of PGC-1α in anabolic pathways is poorly understood. In aged mice, PGC-1α preserves skeletal muscle mass along with Akt and mTOR phosphorylation (15). We have found that mTg CON showed higher p-S6K^{T389} relative levels, while the opposite effect was observed in mKO CON. Interestingly, enhanced oxidative metabolism is associated with increased mTORC1 activity (7, 8), implying that PGC-1α might modulate mTORC1 through its effects on mitochondrial function. Moreover, mTg CON exhibited lower levels of MuRF1 and MSTN mRNA, but neither mTg nor mKO CON showed signs of skeletal muscle hypertrophy, similar to previous reports (16, 28-31). Consistently, we have previously shown that a cluster of genes related to ribosomes and anabolic pathways is down-regulated in mTg skeletal muscle (32). Finally, in vitro, PGC-1α does not regulate the rate of protein synthesis in C_2C_{12} myotubes (14). As a consequence, the assessment of a wide range of parameters related to skeletal muscle hypertrophy revealed that the overall effect of SA was not different in mTg or mKO mice. In fact, endogenous PGC-1α1 and PGC-1α4 were down-regulated by SA in WT mice. Importantly, the fact that both of these coactivators were fully deleted in mKO mice strongly indicates that they are not required for chronic overload-induced skeletal muscle

hypertrophy. In line with these data, PGC-1α overexpression does not overcome skeletal muscle atrophy induced by mTORC1 inhibition via raptor knockout (28). It is important to note that PGC-1α4 was proposed to promote muscle growth via IGF1 and MSTN expression (17), which seem to play a minor role in the context of SA. In fact, even though IGF1 was up-regulated by SA, p-Akt^{T308} relative levels were not increased. Therefore, these data support the concept that mechanical overload-induced skeletal muscle hypertrophy is PI3K-independent (4) and thus might not involve PGC-1α4. Our results do not preclude PGC-1α4 to be required for muscle hypertrophy in other contexts. Accordingly, some studies show no changes in PGC-1α expression in human skeletal muscle following resistance exercise (33-35), while others have reported opposite results (17, 36).

PGC-1α is a central mediator of mitochondrial biogenesis (37). Consistently, concomitantly with a reduction in PGC-1α mRNA, SA strongly repressed the expression and activity of several metabolic-related proteins in both WT and mTg mice. Microarray analysis of human skeletal muscle has also revealed that resistance exercise does not increase the expression of genes involved in oxidative metabolism (38, 39). In fact, resistance-trained athletes exhibit the same (38) or lower relative peak oxygen consumption compared to untrained healthy people (40). These data disagrees with the metabolic role of mTORC1, even though it should be noted that this aspect of mTORC1 function has been mainly studied using genetic and pharmacological approaches. In stark contrast, mechanical overload of skeletal muscle modulates a wide spectrum of signal pathways (1), suggesting that the regulation of additional molecules could blunt the metabolic effects of mTORC1, at least in part via PGC-1α down-regulation.

Interestingly, SA has previously been demonstrated to lower peak force (41, 42), which might be interpreted as a negative effect. However, our data suggest that it actually reflects

an extreme switch to a slow-contractile phenotype. In fact, SA increased the expression of the slow-twitch specific isoform of several genes regulating EC coupling in a PGC-1α-independent way, while the fast-twitch specific isoforms of these genes were concomitantly down-regulated. Importantly, our findings imply that the reduction in peak force induced by SA is mainly related to MyHC-2B, SERCA1, MLCK2 and MLC2 expression. These proteins are highly expressed in fast-twitch muscles and they play a pivotal role in muscle force potentiation (25, 26). In accordance, we found that peak force, MyHC-2B mRNA/protein and MLCK2 mRNA levels were preserved in mKO OVL, while MLC2 protein levels were even increased. Moreover, p-MLC2$^{T18/S19}$ relative levels were higher in mKO mice and the opposite results were observed in mTg CON, supporting thus the effects of PGC-1α on skeletal muscle contractility (29). Interestingly, SA improved fatigue resistance primarily in a PGC-1α-independent way. The metabolic remodeling induced by SA seems to disagree with the functional adaptations. However, our data as well as previous reports (5, 43) show that SA strongly increases AMPK activity and considering its metabolic role (23), it seems likely that AMPK activation compensates for the negative effects of SA on energy metabolism.

In summary, we have now shown that besides inducing skeletal muscle hypertrophy, SA strongly promotes a switch toward a slow-contractile phenotype that seems to be dissociated of the metabolic phenotype. Moreover, we have identified MyHC-2B, MLCK2 and MCL2 as novel PGC-1α targets involved in skeletal muscle contractility. However, our data demonstrates that PGC-1α and PGC-1α4 are not involved in skeletal muscle remodeling induced by chronic overload. In fact, SA seems to disrupt the mTORC1-PGC-1α axis by down-regulation of this coactivator. It should be noted that SA does not fully resemble the effects of resistance exercise in human skeletal muscle in several aspects and therefore, the

relevance of PGC-1α as a therapeutic target aiming at promoting skeletal muscle growth remains to be further explored under different conditions.

Materials and Methods

Animals

Mice were housed in a conventional facility with a 12 h night and day cycle, with free access to food and water. All experiments were performed on adult male mice with approval of the Swiss authorities. Description of mouse generation and genotyping is provided in SI Materials and Methods.

Synergist Ablation

Mechanical overload of plantaris was performed as previously described (43). Briefly, unilateral SA was performed under anesthesia (2.5% isoflurane) and sterile conditions, then soleus and gastrocnemius were surgically removed and animals were allowed to recover for a period of 2 weeks. The contralateral non-operated leg was used as control.

Ex Vivo Assessment of Muscle Function, Histology and Immunohistochemistry, RNA Isolation and Quantitative PCR (qPCR), Protein Isolation and Western Blot, SDH and PFK activity assays

These analyses were performed by standard procedures as described in SI Materials and Methods.

Statistical Analysis

Values are expressed as mean ± standard error of the mean (SEM). Statistical significance was determined with unpaired two-tailed t-tests or one-way ANOVA with Dunnett post-hoc test. Significance was considered with a $p < 0.05$.

ACKNOWLEDGMENTS. We would like to thank Dr. Shuo Lin (Biozentrum, University of Basel) for his help with synergist ablation. This project was funded by by the Swiss National Science Foundation, the Muscular Dystrophy Association USA (MDA), the SwissLife 'Jubiläumsstiftung für Volksgesundheit und medizinische Forschung', the Swiss Society for Research on Muscle Diseases (SSEM), the Swiss Diabetes Association, the Roche Research Foundation, the United Mitochondrial Disease Foundation (UMDF), the Association Française contre les Myopathies (AFM), the Neuromuscular Research Association Basel (NeRAB), the Gebert-Rüf Foundation "Rare Diseases" Program, the University of Basel and the Biozentrum.

References

1. Egan B & Zierath JR (2013) Exercise metabolism and the molecular regulation of skeletal muscle adaptation. (Translated from eng) *Cell Metab* 17(2):162-184 (in eng).

2. Glass D & Roubenoff R (2010) Recent advances in the biology and therapy of muscle wasting. (Translated from eng) *Ann N Y Acad Sci* 1211:25-36 (in eng).

3. von Haehling S, Morley JE, & Anker SD (2012) From muscle wasting to sarcopenia and myopenia: update 2012. (Translated from eng) *J Cachexia Sarcopenia Muscle* 3(4):213-217 (in eng).

4. Philp A, Hamilton DL, & Baar K (2011) Signals mediating skeletal muscle remodeling by resistance exercise: PI3-kinase independent activation of mTORC1. (Translated from eng) *J Appl Physiol* 110(2):561-568 (in eng).

5. Goodman CA*, et al.* (2011) The role of skeletal muscle mTOR in the regulation of mechanical load-induced growth. (Translated from eng) *J Physiol* 589(Pt 22):5485-5501 (in eng).

6. Bentzinger CF*, et al.* (2013) Differential response of skeletal muscles to mTORC1 signaling during atrophy and hypertrophy. (Translated from eng) *Skelet Muscle* 3(1):6 (in eng).

7. Schieke SM*, et al.* (2006) The mammalian target of rapamycin (mTOR) pathway regulates mitochondrial oxygen consumption and oxidative capacity. (Translated from eng) *J Biol Chem* 281(37):27643-27652 (in eng).

8. Ramanathan A & Schreiber SL (2009) Direct control of mitochondrial function by mTOR. (Translated from eng) *Proc Natl Acad Sci U S A* 106(52):22229-22232 (in eng).

9. Duvel K*, et al.* (2010) Activation of a metabolic gene regulatory network downstream of mTOR complex 1. (Translated from eng) *Mol Cell* 39(2):171-183 (in eng).

10. Cunningham JT*, et al.* (2007) mTOR controls mitochondrial oxidative function through a YY1-PGC-1alpha transcriptional complex. (Translated from eng) *Nature* 450(7170):736-740 (in eng).

11. Chaveroux C*, et al.* (2013) Molecular and Genetic Crosstalks between mTOR and ERRalpha Are Key Determinants of Rapamycin-Induced Nonalcoholic Fatty Liver. (Translated from eng) *Cell Metab* 17(4):586-598 (in eng).

12. Blattler SM*, et al.* (2012) Defective mitochondrial morphology and bioenergetic function in mice lacking the transcription factor Yin Yang 1 in skeletal muscle. (Translated from eng) *Mol Cell Biol* 32(16):3333-3346 (in eng).

13. Schiaffino S, Dyar KA, Ciciliot S, Blaauw B, & Sandri M (2013) Mechanisms regulating skeletal muscle growth and atrophy. (Translated from eng) *Febs J* 280(17):4294-4314 (in eng).

14. Brault JJ, Jespersen JG, & Goldberg AL (2010) Peroxisome proliferator-activated receptor gamma coactivator 1alpha or 1beta overexpression inhibits muscle protein degradation, induction of ubiquitin ligases, and disuse atrophy. (Translated from eng) *J Biol Chem* 285(25):19460-19471 (in eng).

15. Wenz T, Rossi SG, Rotundo RL, Spiegelman BM, & Moraes CT (2009) Increased muscle PGC-1alpha expression protects from sarcopenia and metabolic disease during aging. (Translated from eng) *Proc Natl Acad Sci U S A* 106(48):20405-20410 (in eng).

16. Sandri M*, et al.* (2006) PGC-1alpha protects skeletal muscle from atrophy by suppressing FoxO3 action and atrophy-specific gene transcription. (Translated from eng) *Proc Natl Acad Sci U S A* 103(44):16260-16265 (in eng).

17. Ruas JL*, et al.* (2012) A PGC-1alpha isoform induced by resistance training regulates skeletal muscle hypertrophy. (Translated from eng) *Cell* 151(6):1319-1331 (in eng).

18. Bodine SC & Baar K (2012) Analysis of skeletal muscle hypertrophy in models of increased loading. (Translated from eng) *Methods Mol Biol* 798:213-229 (in eng).

19. Lowe DA & Alway SE (2002) Animal models for inducing muscle hypertrophy: are they relevant for clinical applications in humans? (Translated from eng) *J Orthop Sports Phys Ther* 32(2):36-43 (in eng).

20. Handschin C & Spiegelman BM (2011) PGC-1 coactivators and the regulation of skeletal muscle fiber-type determination. (Translated from eng) *Cell Metab* 13(4):351; author reply 352 (in eng).

21. Handschin C*, et al.* (2007) Abnormal glucose homeostasis in skeletal muscle-specific PGC-1alpha knockout mice reveals skeletal muscle-pancreatic beta cell crosstalk. (Translated from eng) *J Clin Invest* 117(11):3463-3474 (in eng).

22. Lin J*, et al.* (2004) Defects in adaptive energy metabolism with CNS-linked hyperactivity in PGC-1alpha null mice. (Translated from eng) *Cell* 119(1):121-135 (in eng).

23. Hardie DG, Ross FA, & Hawley SA (2012) AMPK: a nutrient and energy sensor that maintains energy homeostasis. (Translated from eng) *Nat Rev Mol Cell Biol* 13(4):251-262 (in eng).

24. Schiaffino S & Reggiani C (2011) Fiber types in mammalian skeletal muscles. (Translated from eng) *Physiol Rev* 91(4):1447-1531 (in eng).

25. Drexler HC*, et al.* (2012) On marathons and Sprints: an integrated quantitative proteomics and transcriptomics analysis of differences between slow and fast muscle fibers. (Translated from eng) *Mol Cell Proteomics* 11(6):M111 010801 (in eng).

26. Kamm KE & Stull JT (2011) Signaling to myosin regulatory light chain in sarcomeres. (Translated from eng) *J Biol Chem* 286(12):9941-9947 (in eng).

27. Laplante M & Sabatini DM (2012) mTOR signaling in growth control and disease. (Translated from eng) *Cell* 149(2):274-293 (in eng).

28. Romanino K*, et al.* (2011) Myopathy caused by mammalian target of rapamycin complex 1 (mTORC1) inactivation is not reversed by restoring mitochondrial function. (Translated from eng) *Proc Natl Acad Sci U S A* 108(51):20808-20813 (in eng).

29. Summermatter S*, et al.* (2012) Remodeling of calcium handling in skeletal muscle through PGC-1alpha: impact on force, fatigability, and fiber type. (Translated from eng) *Am J Physiol Cell Physiol* 302(1):C88-99 (in eng).

30. Choi CS*, et al.* (2008) Paradoxical effects of increased expression of PGC-1alpha on muscle mitochondrial function and insulin-stimulated muscle glucose metabolism. (Translated from eng) *Proc Natl Acad Sci U S A* 105(50):19926-19931 (in eng).

31. Handschin C*, et al.* (2007) Skeletal muscle fiber-type switching, exercise intolerance, and myopathy in PGC-1alpha muscle-specific knock-out animals. (Translated from eng) *J Biol Chem* 282(41):30014-30021 (in eng).

32. Perez-Schindler J*, et al.* (2012) The corepressor NCoR1 antagonizes PGC-1alpha and estrogen-related receptor alpha in the regulation of skeletal muscle function and oxidative metabolism. (Translated from eng) *Mol Cell Biol* 32(24):4913-4924 (in eng).

33. Coffey VG*, et al.* (2006) Early signaling responses to divergent exercise stimuli in skeletal muscle from well-trained humans. (Translated from eng) *Faseb J* 20(1):190-192 (in eng).

34. Item F*, et al.* (2013) Combined whole-body vibration, resistance exercise, and sustained vascular occlusion increases PGC-1alpha and VEGF mRNA abundances. (Translated from eng) *Eur J Appl Physiol* 113(4):1081-1090 (in eng).

35. Donges CE*, et al.* (2012) Concurrent resistance and aerobic exercise stimulates both myofibrillar and mitochondrial protein synthesis in sedentary middle-aged men. (Translated from eng) *J Appl Physiol* 112(12):1992-2001 (in eng).

36. Apro W, Wang L, Ponten M, Blomstrand E, & Sahlin K (2013) Resistance exercise induced mTORC1 signaling is not impaired by subsequent endurance exercise in human skeletal muscle. (Translated from eng) *Am J Physiol Endocrinol Metab* 305(1):E22-32 (in eng).

37. Pérez-Schindler J & Handschin C (2013) New insights in the regulation of skeletal muscle PGC-1α by exercise and metabolic diseases. *Drug Discovery Today: Disease Models* 10(2):e79-e85.

38. Stepto NK*, et al.* (2009) Global gene expression in skeletal muscle from well-trained strength and endurance athletes. (Translated from eng) *Med Sci Sports Exerc* 41(3):546-565 (in eng).

39. Liu D*, et al.* (2010) Skeletal muscle gene expression in response to resistance exercise: sex specific regulation. (Translated from eng) *BMC Genomics* 11:659 (in eng).

40. Salvadego D*, et al.* (2013) Skeletal muscle oxidative function in vivo and ex vivo in athletes with marked hypertrophy from resistance training. (Translated from eng) *J Appl Physiol* 114(11):1527-1535 (in eng).

41. Kandarian SC & White TP (1989) Force deficit during the onset of muscle hypertrophy. (Translated from eng) *J Appl Physiol* 67(6):2600-2607 (in eng).

42. Kandarian SC & White TP (1990) Mechanical deficit persists during long-term muscle hypertrophy. (Translated from eng) *J Appl Physiol* 69(3):861-867 (in eng).

43. McGee SL, Mustard KJ, Hardie DG, & Baar K (2008) Normal hypertrophy accompanied by phosphoryation and activation of AMP-activated protein kinase alpha1 following overload in LKB1 knockout mice. (Translated from eng) *J Physiol* 586(6):1731-1741 (in eng).

Figure legends

Fig. 1. Effects of SA on Plantaris Hypertrophy. (A) Relative plantaris weight (n = 15-18 per group). (B and C) Absolute and relative plantaris protein levels (n = 6 per group). (D) Whole plantaris CSA (n = 3 per group). (E and F) Representative pictures of laminin staining and quantification of fiber CSA (n = 3 per group). (G) Western blot analysis of mTORC1 and PI3K target proteins (n = 6 per group). (H and I) qPCR analysis of pro-hypertrophic and pro-atrophic genes (n = 6 per group). Values are mean ± SEM. *p < 0.05, **p < 0.01, ***p < 0.001.

Fig. 2. Plantaris Metabolism is Repressed by SA. (A) qPCR analysis of metabolic-related genes (n = 6 per group). (B) Western blot analysis of different components of the ETC (n = 6 per group). (C and D) SDH and PFK activity assessment (n = 6 per group). (E) Representative pictures of NADH staining (n = 3 per group). (F) qPCR analysis of PGC-1 family of coactivators (n = 6 per group). (G) Western blot analysis of AMPK activation (n = 6 per group). Values are mean ± SEM. *p < 0.05, **p < 0.01, ***p < 0.001.

Fig. 3. Effects of SA on Plantaris Contractility. (A-C) Peak force in response to a single twitch or tetanic stimulation (n = 5-6 per group). (D-F) Assessment of fatigue resistance and the corresponding AUC (n = 5-6 per group). Values are mean ± SEM. *p < 0.05, **p < 0.01, ***p < 0.001. In D and E *p < 0.05 CON vs. OVL WT, $^{\#}$p < 0.05 CON vs. OVL mTg or mKO, §p < 0.05 CON WT vs. mTg or mKO.

Fig. 4. SA Modulates the Expression of EC Coupling-Related Genes. (A-F) qPCR and Western blot analysis of key regulators of EC coupling in plantaris (Arrow head indicates MLC2; n = 6 per group). Values are mean ± SEM. *p < 0.05, **p < 0.01, ***p < 0.001.

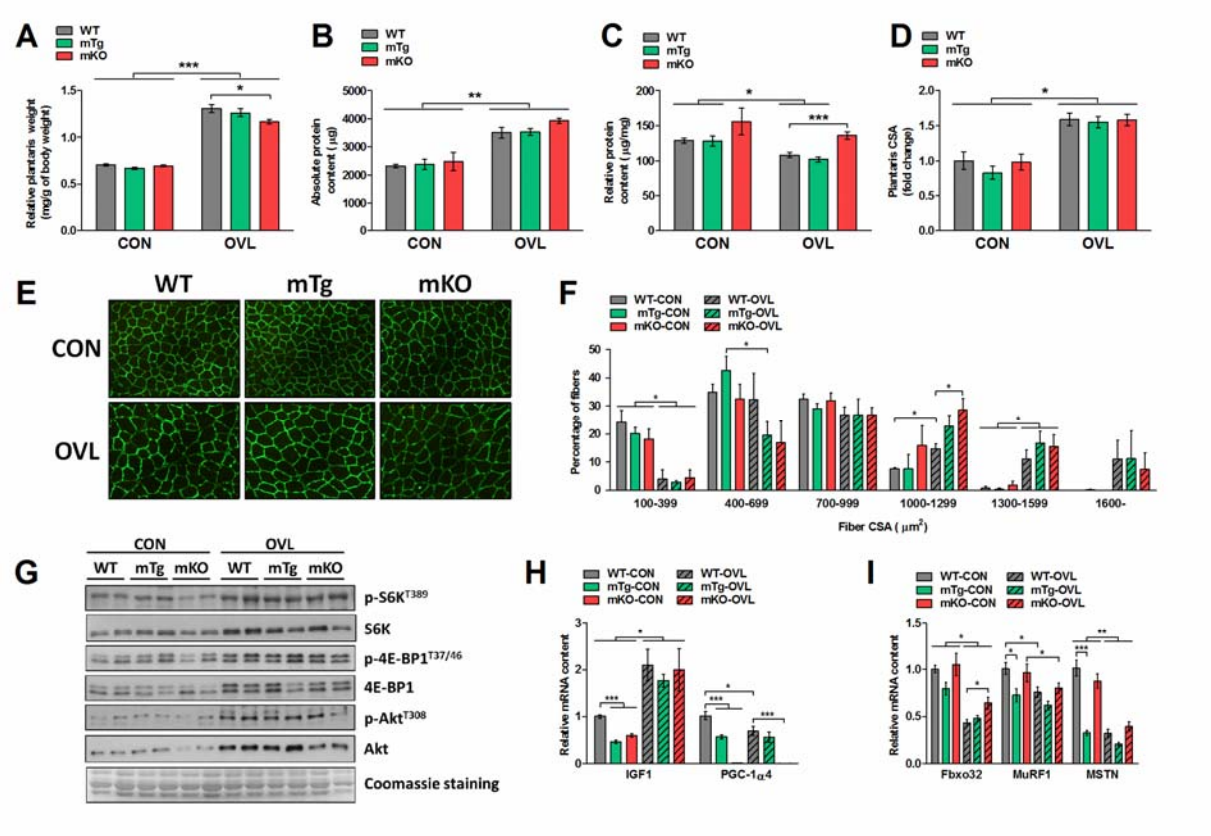

Fig. 1. Effects of SA on Plantaris Hypertrophy. (A) Relative plantaris weight (n = 15-18 per group). (B and C) Absolute and relative plantaris protein levels (n = 6 per group). (D) Whole plantaris CSA (n = 3 per group). (E and F) Representative pictures of laminin staining and quantification of fiber CSA (n = 3 per group). (G) Western blot analysis of mTORC1 and PI3K target proteins (n = 6 per group). (H and I) qPCR analysis of pro-hypertrophic and pro-atrophic genes (n = 6 per group). Values are mean ± SEM. *p < 0.05, **p < 0.01, ***p < 0.001.

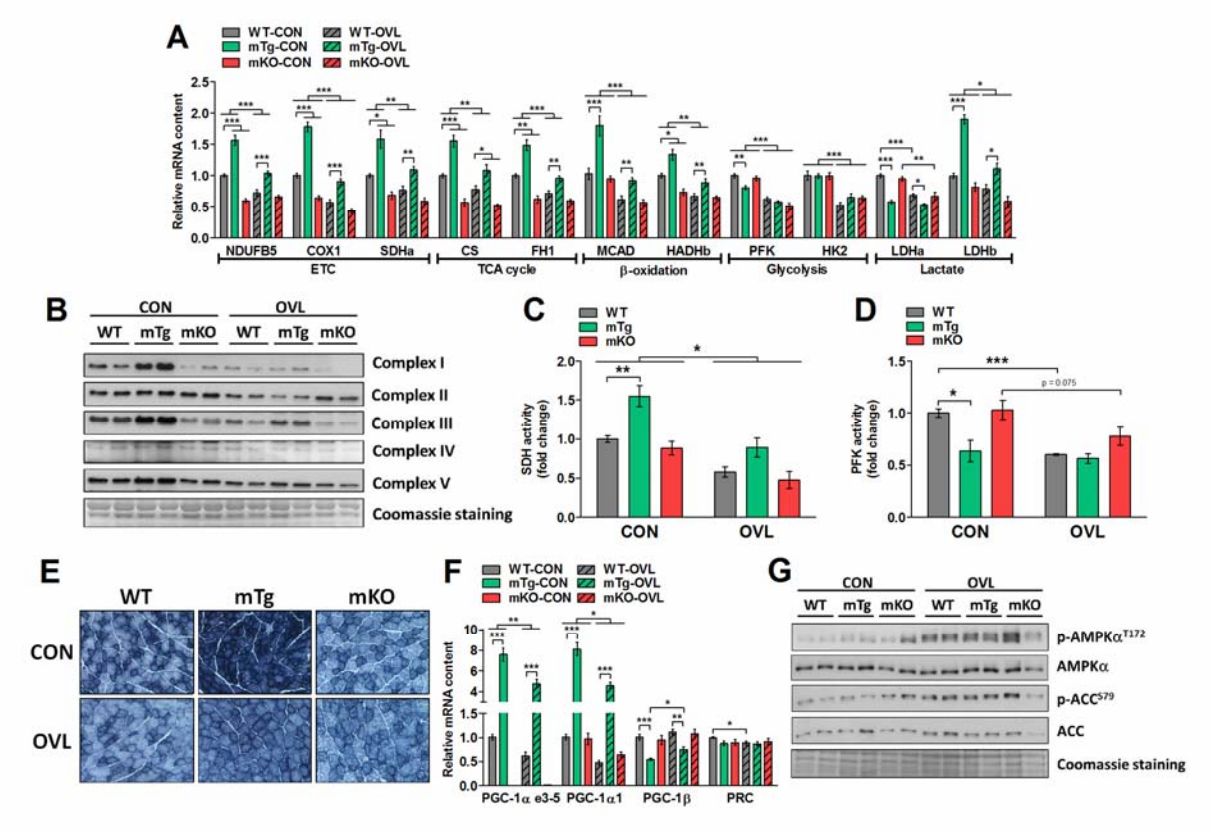

Fig. 2. Plantaris Metabolism is Repressed by SA. (A) qPCR analysis of metabolic-related genes (n = 6 per group). (B) Western blot analysis of different components of the ETC (n = 6 per group). (C and D) SDH and PFK activity assessment (n = 6 per group). (E) Representative pictures of NADH staining (n = 3 per group). (F) qPCR analysis of PGC-1 family of coactivators (n = 6 per group). (G) Western blot analysis of AMPK activation (n = 6 per group). Values are mean ± SEM. *p < 0.05, **p < 0.01, ***p < 0.001.

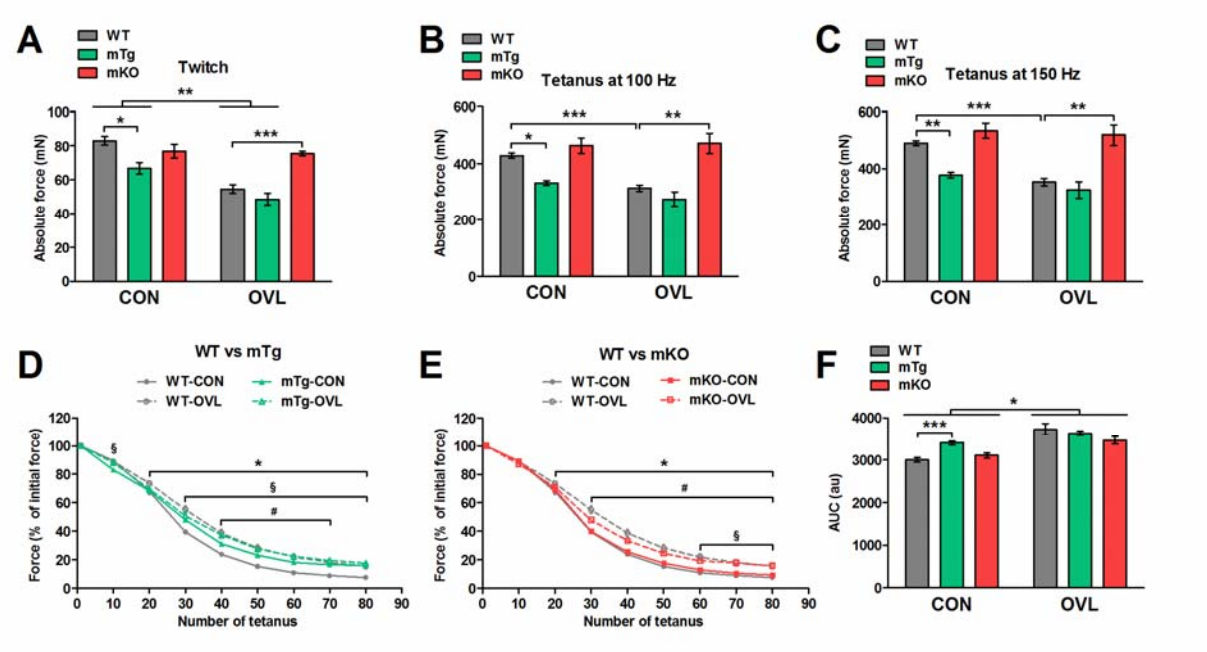

Fig. 3. Effects of SA on Plantaris Contractility. (A-C) Peak force in response to a single twitch or tetanic stimulation (n = 5-6 per group). (D-F) Assessment of fatigue resistance and the corresponding AUC (n = 5-6 per group). Values are mean ± SEM. *p < 0.05, **p < 0.01, ***p < 0.001. In D and E *p < 0.05 CON vs. OVL WT, $^{\#}$p < 0.05 CON vs. OVL mTg or mKO, §p < 0.05 CON WT vs. mTg or mKO.

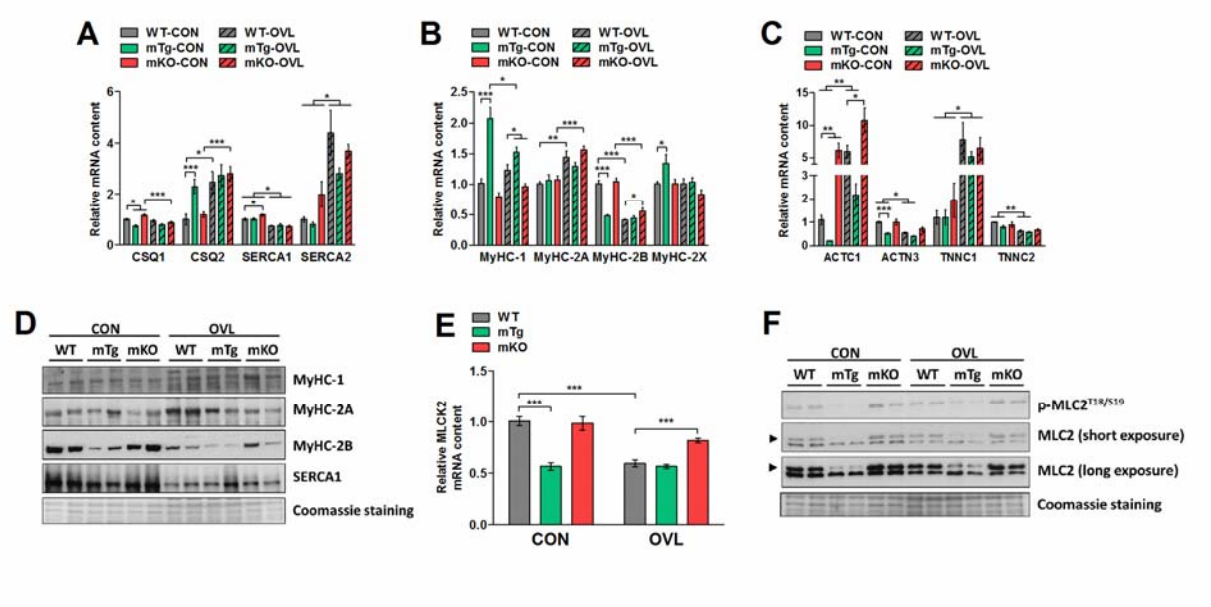

Fig. 4. SA Modulates the Expression of EC Coupling-Related Genes. (A-F) qPCR and Western blot analysis of key regulators of EC coupling in plantaris (Arrow head indicates MLC2; n = 6 per group). Values are mean ± SEM. *p < 0.05, **p < 0.01, ***p < 0.001.

Supporting Information

SI Material and Methods

Animals

PGC-1α muscle-specific transgenic (mTg) mice were generated by expressing PGC-1α transgene under the control of the MCK promoter as previously described (1). On the other hand, PGC-1α muscle-specific knockout (mKO) mice were generated by crossing PGC-1α$^{loxP/loxP}$ mice with HSA-Cre transgenic mice. PGC-1α$^{loxP/loxP}$ mice were generated as previously described (2). The genotype of mTg and mKO animals was assessed by PCR using specific primer pairs to detect the presence of the PGC-1α transgene, 5' loxP site and recombination of the PGC-1α floxed allele in heart, quadriceps and tibialis anterior (Fig. S1A). To further confirm the genotypes, qPCR analysis of these tissues was performed, revealing a ~10 fold increase and full deletion of PGC-1α mRNA in skeletal muscle of mTg and mKO mice, respectively (Fig. S1B).

Ex Vivo Assessment of Muscle Function

Proximal tendon of plantaris was left inserted into the distal femoral stub. The femur stub and the distal tendon were then ligated to silk and mounted onto Muscle Tester chamber (SI-Heidelberg, Germany). Muscles were stimulated by supra-maximal electrical field pulses of 0.5 ms duration via platinum electrodes. After determining the optimal length, isometric twitch and tetanic force were recorded at 4 kHz with Power Lab AD Instruments converter. Tetanic contraction was assessed by stimulating the muscles for 800 ms with train of pulses of 0.5 ms duration delivered at 100 Hz or 150 Hz. After tetanic stimulation, the muscle rested for 10 min. Fatigue resistance was assessed in response to train of 100 Hz tetani of 400 ms duration delivered at 0.27 Hz for 5 min. Changes in force generation during the fatigue protocol are expressed as percentage of initial force.

Histology and Immunohistochemistry

NADH staining was performed on 12 μm cross sections from plantaris by exposing them to 0.8 mg/mL NADH in the presence of 1 mg/mL nitro blue tetrazolium.

For immunohistochemistry, 10 μm cross sections from plantaris were fixed in 100% methanol for 6 min, rinsed 2 times with 0.1 M glycine in PBS pH 6.8 and subsequently microwave antigen retrieval was performed using 0.01 M citric acid pH 6.0. After rinsing with PBS, sections were blocked in 3% BSA in PBS for 1 h at room temperature, rinsed with PBS and then incubated overnight with laminin antibody (Abcam #ab11575) in 3% BSA in PBS (1:500 dilution). The following day, sections were rinsed 3 times with PBS and incubated with appropriated secondary antibody (Invitrogen #A-11008) in 3% BSA in PBS (1:500 dilution) for 1.5 h at room temperature. Finally, sections were rinsed 3 times with PBS and mounted using Vectashield medium (Vector #H-1500). Images were acquired with a fluorescent microscope (Leica) and analyzed using the analySIS software (Soft Imaging System). Muscle fiber CSA was quantified according to standard procedures as previously described (3).

RNA Isolation and Quantitative PCR (qPCR)

Total RNA was isolated from heart, plantaris, tibialis anterior and quadriceps from WT, mTg and mKO mice using lysing matrix tubes (MP Biomedicals) and TRI Reagent® (Sigma-Aldrich) according to the manufacturer's instructions. RNA concentration was measured with a NanoDrop 1000 spectrophotometer (Thermo Scientific). One microgram of RNA was treated with DNase I (Invitrogen) and then reversed transcribed using hexanucleotide mix (Roche) and SuperScript™ II reverse transcriptase (Invitrogen). Relative mRNA was quantified by qPCR on a StepOnePlus system (Applied Biosystems) using Power SYBR® Green PCR Master Mix (Applied Biosystems). The sequences of the qPCR primers are depicted in Supplemental Table S3. Specific primers for PGC-1α1 and PGC-1α4 have been previously reported (4).

Analysis was performed by the $\Delta\Delta C_T$ method using TATA binding protein (TBP) as endogenous control. TBP transcript levels were not different between genotypes or different experimental conditions.

Protein Isolation and Western Blot

Plantaris was powdered on dry ice and homogenized in 300 µL of ice-cold lysis buffer (50 mM Tris-HCl pH 7.5, 250 mM Sucrose, 1 mM EDTA, 1 mM EGTA, 0.25% Nonidet P 40 substitute, 50 mM NaF, 5 mM $Na_4P_2O_7$, 0.1% DTT, fresh protease and phosphatase inhibitor cocktail). Then, samples were shaken at 1300 rpm for 30 min at 4°C. Samples were subsequently centrifuged at 13000 g for 10 min at 4°C and the protein concentration of the supernatant determined by the Bradford assay (Bio-Rad). Equal aliquots of protein were boiled for 5 min in Laemmli sample buffer (250 mM Tris-HCl pH 6.8, 2% SDS, 10% glycerol, 0.01% bromophenol blue and 5% β-mercaptoetanol).

Samples were separated on SDS-polyacrylamide gels and then transferred to nitrocellulose membranes for 1 h. Membranes were blocked for 1 h in 3% milk in Tris-buffered saline and 0.1% tween-20 (TBST) before overnight incubation at 4°C with appropriate primary antibody in TBST (1:1000 dilution). Proteins were detected with a primary antibody to S6K (Cell Signaling #2708), p-S6K^{T389} (Cell Signaling #9206), 4E-BP1 (Cell Signaling #9644), p-4E-BP1$^{T37/46}$ (Cell Signaling #2855), Akt (Cell Signaling #9272), p-Akt^{T308} (Cell Signaling #4056), AMPKα (Cell Signaling #2603), p-AMPKα^{T172} (Cell Signaling #2535), ACC (Cell Signaling #3662), p-ACC^{S79} (Cell Signaling #3661), MLC2 (Cell Signaling #3672), p-MLC2$^{T18/S19}$ (Cell Signaling #3674), SERCA1 (Cell Signaling #4219) and total OXPHOS (Abcam #ab110413). The MyHC-1 (BA-F8), MyHC-2A (SC-71) and MyHC-2B (BF-F3) antibodies developed by Dr. Stefano Schiaffino (Venetian Institute of Molecular Medicine, Italy) were obtained from the Developmental Studies Hybridoma Bank developed under the auspices of the NICHD and

maintained by The University of Iowa, Department of Biology, Iowa City, IA 52242. Coomassie staining was used as loading control by using SimplyBlue™ SafeStain (Invitrogen: lc6060). Following incubation, membranes were washed 3 times with TBST before incubation with an appropriate peroxidase-conjugated secondary (Dako) antibody in TBST (1:10000 dilution). Antibody binding was detected using enhanced chemiluminescence HRP substrate detection kit (Pierce: 32106) and quantified using ImageJ program.

Succinate dehydrogenase (SDH) and phosphofructokinase (PFK) activity assays

SDH and PFK enzymatic activities were determined colorimetrically by incubating 50 µL of protein extracts (50 µg of protein) with 50 µL of SDH assay buffer (50 mM sodium succinate, 0.5 mg/mL nitro blue tetrazolium, 0.03 mg/mL phenazine methosulfate and 50 mM sodium phosphate buffer pH 7.6) or PFK assay buffer (2 mM D-fructose 6-phosphate, 1 mM β-NAD, 1 mM ATP, 1 mM magnesium sulfate, 0.4 mg/mL nitro blue tetrazolium, 0.03 mg/mL phenazine methosulfate and 10 mM sodium arsenate pH 7.4) at 37°C for 10-70 min. A second set of samples was incubated in background control solution without substrate (sodium succinate or D-fructose 6-phosphate) in order to measure endogenous NADH oxidation. Background values were subtracted for further analysis. Absorbance at 450 nm was measured at two different time points and the difference was used to calculate relative enzymatic activity.

SI Figure and Table Legends

Fig. S1. Determination of Genotypes and Hypertrophic Effects of SA. (A) Detection of PGC-1α transgene, 5' loxP site and recombination of the PGC-1α floxed allele from genomic DNA via PCR genotyping in heart, quadriceps (QUA) and tibialis anterior (TA) of WT, mTg and mKO mice. (B) qPCR analysis of total PGC-1α mRNA levels (exons 3 to 5) in heart, QUA and TA of WT, mTg and mKO mice (n = 6 per group). (C and D) Absolute and relative plantaris RNA levels (n = 6 per group). (E and F) Western blot quantification of phosphorylation and total protein content of mTORC1 and PI3K target proteins (n = 6 per group). Values are mean ± SEM. *p < 0.05, **p < 0.01, ***p < 0.001.

Fig. S2. Metabolic Effects of SA. (A) qPCR analysis of metabolic-related genes (n = 6 per group). (B) Western blot quantification of different components of the ETC (n = 6 per group). (C) Changes in average CSA of positive, negative and all fibers assessed by NADH staining (n = 3 per group). (D and E) Western blot quantification of AMPK activity (n = 6 per group). Values are mean ± SEM. *p < 0.05, **p < 0.01, ***p < 0.001. In D *p < 0.05, **p < 0.01 vs. CON.

Fig. S3. SA Decreases Plantaris Contractility. (A-C) Western blot quantification of total protein content of MyHC-1, MyHC-2A, MyHC-2B, SERCA1, p-MLC2$^{T18/S19}$ and MLC2 (n = 6 per group). Values are mean ± SEM. *p < 0.05, **p < 0.01, ***p < 0.001.

Table S1. Body and Muscle Weight of WT, mTg and mKO Mice

Table S2. Contractile Kinetics of Plantaris from WT, mTg and mKO Mice

Table S3. qPCR Primers sequences

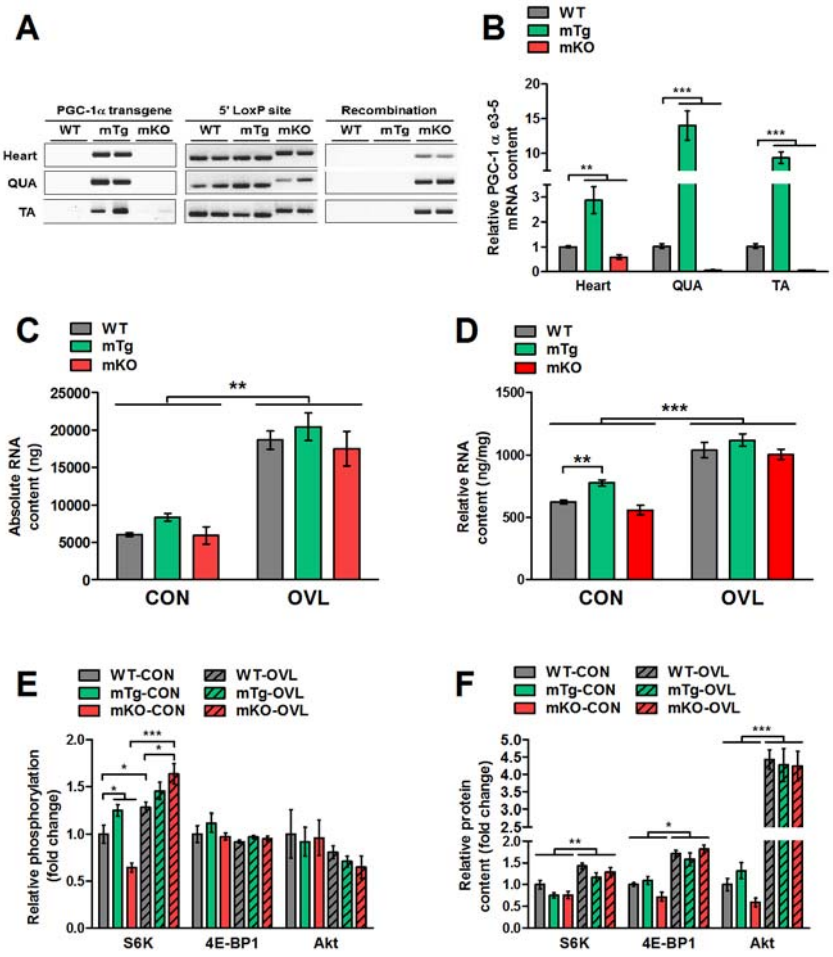

Supplemental Figure S1. Determination of Genotypes and Hypertrophic Effects of SA. (A) Detection of PGC-1α transgene, 5' loxP site and recombination of the PGC-1α floxed allele from genomic DNA via PCR genotyping in heart, quadriceps (QUA) and tibialis anterior (TA) of WT, mTg and mKO mice. (B) qPCR analysis of total PGC-1α mRNA levels (exons 3 to 5) in heart, QUA and TA of WT, mTg and mKO mice (n = 6 per group). (C and D) Absolute and relative plantaris RNA levels (n = 6 per group). (E and F) Western blot quantification of phosphorylation and total protein content of mTORC1 and PI3K target proteins (n = 6 per group). Values are mean ± SEM. *p < 0.05, **p < 0.01, ***p < 0.001.

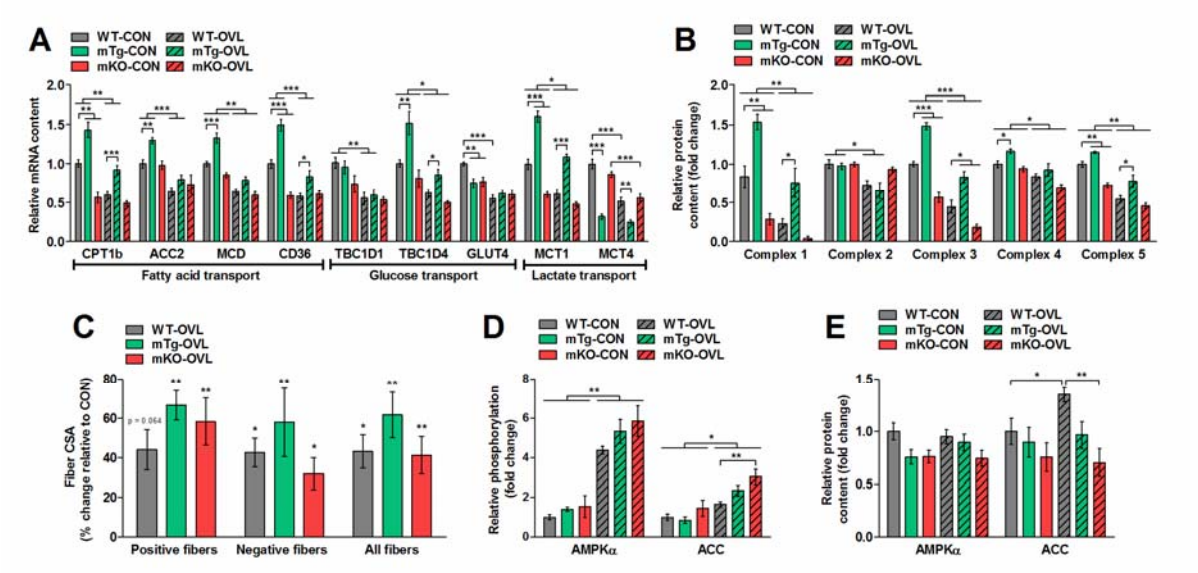

Supplemental Figure S2. Metabolic Effects of SA. (A) qPCR analysis of metabolic-related genes (n = 6 per group). (B) Western blot quantification of different components of the ETC (n = 6 per group). (C) Changes in average CSA of positive, negative and all fibers assessed by NADH staining (n = 3 per group). (D and E) Western blot quantification of AMPK activity (n = 6 per group). Values are mean ± SEM. *p < 0.05, **p < 0.01, ***p < 0.001. In D *p < 0.05, **p < 0.01 vs. CON.

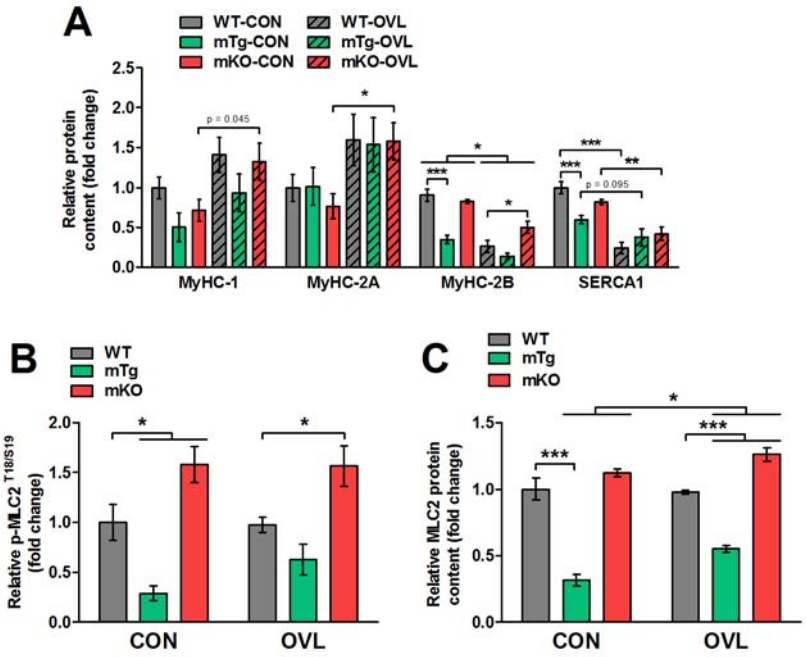

Supplemental Figure S3. SA Decreases Plantaris Contractility. (A-C) Western blot quantification of total protein content of MyHC-1, MyHC-2A, MyHC-2B, SERCA1, p-MLC2$^{T18/S19}$ and MLC2 (n = 6 per group). Values are mean ± SEM. *p < 0.05, **p < 0.01, ***p < 0.001.

Table S1 Body and Muscle Weight of WT, mTg and mKO Mice

Weight	WT	mTg	mKO
Body weight (g)	25.5 ± 0.21	26.8 ± 0.58	25.7 ± 0.27
Gastrocnemius (mg)	141.3 ± 2.24	139.0 ± 4.17	139.3 ± 2.51
Soleus (mg)	9.4 ± 0.19	10.5 ± 0.36*	9.7 ± 0.29
Plantaris (mg)	18.9 ± 0.42	18.3 ± 0.62	18.0 ± 0.29
Tibialis anterior (mg)	50.2 ± 0.70	47.1 ± 1.29	47.3 ± 0.77
Extensor digitorum longus (mg)	11.4 ± 0.14	10.2 ± 0.38**	9.8 ± 0.18***
Quadriceps (mg)	232.8 ± 3.08	222.7 ± 7.29	215.8 ± 3.84

Values are mean ± SEM (n = 10-25 per group). *p < 0.05, **p < 0.01, ***p < 0.001 vs. WT.

Table S2 Contractile Kinetics of Plantaris from WT, mTg and mKO Mice

	CON			OVL		
Twitch	**WT**	**mTg**	**mKO**	**WT**	**mTg**	**mKO**
TTP (ms)	14.8 ± 0.7	13.9 ± 0.3	13.9 ± 0.7	12.7 ± 0.3*	12.6 ± 0.4*	12.8 ± 0.4
½TTP (ms)	4.3 ± 0.2	4.2 ± 0.2	4.2 ± 0.2	4.1 ± 0.1	3.8 ± 0.1	4.1 ± 0.2
½RT (ms)	16.6 ± 1.1	16.4 ± 2.6	13.8 ± 1.9	17.0 ± 1.2	13.3 ± 1.5	12.1 ± 1.0$^{\#}$
Tetanus 100 Hz						
½CT (ms)	29.4 ± 2.0	30.4 ± 0.8	27.6 ± 1.4	36.6 ± 2.2*	36.3 ± 1.1**	36.8 ± 2.4*
½RT (ms)	22.9 ± 0.3	20.8 ± 0.7	25.8 ± 1.1	29.8 ± 0.9***	23.6 ± 0.5$^{*,\#\#\#}$	34.6 ± 0.8$^{***,\#\#}$
Tetanus 150 Hz						
½CT (ms)	23.3 ± 0.7	26.1 ± 0.2	25.4 ± 1.2	27.9 ± 1.7*	28.1 ± 1.3	28.9 ± 1.4
½RT (ms)	27.6 ± 0.6	23.0 ± 0.3$^{\#\#\#}$	29.0 ± 0.8	36.6 ± 1.1***	28.2 ± 0.7$^{***,\#\#\#}$	39.8 ± 0.8***

TTP: time to peak, ½TTP: half time to peak, ½RT: half relaxation time, ½CT: half contraction time. Values are mean ± SEM (n = 5-6 per group). *p < 0.05, **p < 0.01, ***p < 0.001 CON vs. OVL; $^{\#}$p < 0.05, $^{\#\#}$p < 0.01, $^{\#\#\#}$p < 0.001 vs. WT of the same group.

Table S3 qPCR Primer sequences

Target gene	Forward primer	Reverse primer
IGF1	CTGGACCAGAGACCCTTTGC	CCTCGGTCCACACACGAACT
Fbxo32	AAAGCCCTCTCTTGGTTCTGACT	GAGAAGAGGTGCAGGGACTGA
MuRF1	AGGCAGCCACCCGATGT	TCACACGTGAGACAGTAGATGTTGA
MSTN	GCTGGCCCAGTGGATCTAAA	GCCCCTCTTTTTCCACATTTT
NDUFB5	TTTTCTCACGCGGAGCTTTC	TGCCATGGTCCCCACTGT
COX1	TGCTAGCCGCAGGCATTACT	GCGGGATCAAAGAAAGTTGTG
SDHa	GCTGGTGTGGATGTCACTAAGG	CCCACCCATGTTGTAATGCA
CS	CCCAGGATACGGTCATGCA	GCAAACTCTCGCTGACAGGAA
FH1	TGCTCTCAGTGCAAAATCCAA	CGTGTGAGTTCGCCCAATT
MCAD	AACACTTACTATGCCTCGATTGCA	CCATAGCCTCCGAAAATCTGAA
HADHb	TGCTGTCAGGCACTTCGTATAAA	AAACCCGAAAGTGCAGCTCTAG
PFK	TGTGGTCCGAGTTGGTATCTT	GCACTTCCAATCACTGTGCC
HK2	CCCTGCCACCAGACGAAA	GACTTGAACCCCTTAGTCCATGA
LDHa	CATTGTCAAGTACAGTCCACACT	TTCCAATTACTCGGTTTTTGGGA
LDHb	CATTGCGTCCGTTGCAGATG	GGAGGAACAAGCTCCCGTG
CPT1b	ATCATGTATCGCCGCAAACT	CCATCTGGTAGGAGCACATGG
ACC2	GGGCTCGGGCATGATTG	CAGGTAAGCCCCGATTCCA
MCD	ACTCCATCAGCCTGACCCAG	ACCCCTTGAGGCTCTCGTGA
CD36	GGCAAAGAACAGCAGCAAAAT	TGGCTAGATAACGAACTCTGTATGTGT
TBC1D1	CATAAAGAACACACTCCCCAACCT	TGCTTGGCGATGTCCATCT
TBC1D4	GTACCGACCGGATATGATGTCA	CGGTGGTAGTCATGAAGGAGTCT
GLUT4	CATGGCTGTCGCTGGTTTC	AAACCCATGCCGACAATGA
MCT1	GTGACCATTGTGGAATGCTG	CTCCGCTTTCTGTTCTTTGG
MCT4	TCACGGGTTTCTCCTACGC	GCCAAAGCGGTTCACACAC
PGC-1α e3-5	AGCCGTGACCACTGACAACGAG	GCTGCATGGTTCTGAGTGCTAAG
PGC-1β	CCATGCTGTTGATGTTCCAC	GACGACTGACAGCACTTGGA
PRC	CACCCTGCCGGAGTGAAAT	CGCATTGACTGCTGCTTGTC
CSQ1	ACTCAGAGAAGGATGCAGCT	CTCTACAGGGTCTTCTAGGA
CSQ2	AGCTTGTGGAGTTTGTGAAG	GGATTGTCAGTGTTGTCCC
SERCA1	AGCCAGTGATGGAGAACTCG	CACCACCAACCAGATGTCAG
SERCA2	GAGAACGCTCACACAAAGACC	CAATTCGTTGGAGCCCCAT
MyHC-1	CCTCCTCACATCTTCTCCATCTCT	TGGACTGATTCTCCCGATCTG
MyHC-2A	CCCCGCCCCACATCTT	TGACTGATTCTCCCTGTCTGTTAGC
MyHC-2B	CAACCCATATGACTTTGCTTACGT	TCCCAGGATATCAACAGCAGTGT
MyHC-2X	GGCCCCACCCCACATC	CTCCCGATCTGTCAGCATGA
ACTC1	CACCACTGCTGAACGTGAAATT	TCCAGGGCGACGTAACACA
ACTN3	AGGAGCAGCTCAACGAATTCC	TCGTCGGGCTCCATCATC
TNNC1	GGCACAGTGGACTTCGATGA	TTCCCTTTGCTGTCGTCCTT
TNNC2	AAAGAGTTGGGCACCGTGAT	GGCATCCAATTCCTCTTTGG
MLCK2	AGCCAAGGTCATCAAGAAACAGA	GACCTCGATCTCCAGCAACAC

SI References

1. Lin J*, et al.* (2002) Transcriptional co-activator PGC-1 alpha drives the formation of slow-twitch muscle fibres. *Nature* 418(6899):797-801.
2. Lin J*, et al.* (2004) Defects in adaptive energy metabolism with CNS-linked hyperactivity in PGC-1alpha null mice. *Cell* 119(1):121-135.
3. Bodine SC & Baar K (2012) Analysis of skeletal muscle hypertrophy in models of increased loading. *Methods Mol Biol* 798:213-229.
4. Ruas JL*, et al.* (2012) A PGC-1alpha isoform induced by resistance training regulates skeletal muscle hypertrophy. *Cell* 151(6):1319-1331.